Observation of diffraction cancellation for nonparaxial beams in the scale-free-optics regime

F. Di Mei,[1,2] D. Pierangeli,[1] J. Parravicini,[1] C. Conti,[3,1] A. J. Agranat,[4] and E. DelRe[1,3,*]

[1]*Dipartimento di Fisica, Università di Roma "La Sapienza," 00185 Rome, Italy*

[2]*Center for Life Nanoscience at Sapienza, Istituto Italiano di Tecnologia, 00161 Rome, Italy*

[3]*ISC-CNR, Università di Roma "La Sapienza," 00185 Rome, Italy*

[4]*Brojde Center for Innovative Engineering and Computer Science, Hebrew University, Jeruslaem 91904, Israel*

(Received 27 March 2015; published 22 July 2015)

We report the observation of diffraction cancellation for visible beams with widths from tens of wavelengths down to fractions of the optical wavelength. The phenomenon is observed at the transition from diffraction- to antidiffraction-dominated beam propagation, triggered by a thermal shock in a photorefractive nanodisordered lithium-enriched potassium-tantalate-niobate (KTN:Li) crystal. Here beams propagate without distortion, independently of intensity and size. Confirming the main prediction of the scale-free-optics model, we find a single unified light behavior that spans across the entire hierarchy of standard optical spatial scales, from wide plane-wave-like beams that obey geometrical optics down to ultranarrow beams with widths of the order of a single wavelength.

DOI: 10.1103/PhysRevA.92.013835 PACS number(s): 42.25.Fx, 42.65.Jx

I. INTRODUCTION

Light beams confined to widths comparable to their wavelength are no longer described by ray optics and diffraction. Light spreads during propagation with an angle that is proportional to the ratio between the wavelength λ and the transverse size of the beam w_0, i.e., $\Delta\theta \sim (w_0/\lambda)^{-1}$ [1,2]. Diffraction can be canceled in the periodic index of refraction patterns [3–5], electromagnetically induced transparency [6], and in systems supporting scale-free optics [7]. The problem with all these approaches is that they are limited to paraxial conditions, where $\Delta\theta \ll 1$ and diffraction causes only limited distortion. Theoretical models indicate that, in principle, scale-free optics supported by the diffusive nonlinearity [8–11] should allow diffraction cancellation also in the nonparaxial regime [12]. This is expected to occur as long as a material-dependent diffusive length scale $L = \lambda$, but to date no experimental verification in the $\Delta\theta \sim 1$ has been provided [13–15].

Here we report the first observation of scale-free propagation across the entire range of possible propagating beam widths, from plane waves to nonparaxial waves, for $w_0/\lambda =$ 0.8–20. To fulfill the scale-free condition in the nonparaxial regime we make use of the recently discovered transition from diffractive to antidiffractive optics when the supporting ferroelectric, a photorefractive nanodisordered ferroelectric KTN:Li, is subject to a thermal shock [16]. Most importantly, this transition has been observed for nonparaxial and even subwavelength beams [17]. The thermal shock causes a transient $L(t)$, and as the beams pass from diffracting ($L < \lambda$) to antidiffracting ($L > \lambda$), they naturally enter the scale-free regime ($L = \lambda$).

II. NONPARAXIAL SCALE-FREE OPTICS

According to the macroscopic Maxwell equations, a linearly polarized optical field $\mathbf{E} = \hat{\mathbf{x}}E\exp(ik_z z)$ propagating inside an inhomogeneous transparent material of index of refraction n obeys the Helmholtz equation

$$\nabla^2 E + (\omega n/c)^2 E = 0, \tag{1}$$

the basic wave equation $\nabla \wedge \nabla \wedge \mathbf{E} = (\omega n/c)^2\mathbf{E}$, where coherent vectorial coupling is neglected ($\nabla\nabla \cdot \mathbf{E} \simeq 0$). Here ω is the optical angular frequency and c is the speed of light in a vacuum (i.e., $2\pi/\lambda = \omega/c$). Light-matter interaction is described by a light-induced change in the index of refraction Δn, so that $n = n_0 + \Delta n$. Specifically, in a nanodisordered photorefractive crystal, light absorbed by deep in-band impurities promotes conduction electrons that diffuse and give rise to a static electric field $\mathbf{E}_{dc} = -(k_B T/q)\nabla I/I$, where k_B is the Boltzmann constant, T is the crystal temperature, q is the elementary charge, $I = |E|^2$ is the optical intensity, and A is the optical field amplitude. When the sample is above its dielectric peak temperature T_m [18], the electro-optic response is dominated by so-called polar nanoregions (PNRs) [19] that give rise to a scalar change $\Delta n = -(n_0^3/2)g\epsilon_0^2\chi_{PNR}^2|\mathbf{E}_{dc}|^2$ [14] where ε_0 is the vacuum dielectric permittivity, χ_{PNR} is the PNR low-frequency susceptibility, and g is the electro-optic coefficient. The Helmholtz equation for this diffusive nonlinearity reads [12]

$$-\frac{\nabla^2 E}{E} + \left(\frac{L}{\lambda}\right)^2\left(\frac{\nabla|E|^2}{2|E|^2}\right)^2 = k^2, \tag{2}$$

where the characteristic length $L = 4\pi n_0^2\varepsilon_0\sqrt{g}\chi_{PNR}(k_B T/q)$ is introduced, and $k = 2\pi n_0/\lambda$. The scale-free condition holds when $L = \lambda$ for which the Helmholtz equation, Eq. (2), retains a trace of λ only in the constant in the right-hand side (RHS). In this case, one has the solution $E = E_0\exp(-(x^2+y^2)/w_0^2)\exp(-ik_z z)$, which is scale free; i.e., it forms for an arbitrary amplitude A_0 and waist w_0, with

$$k_z = \sqrt{\left(\frac{\omega n_0}{c}\right)^2 - \frac{4}{w_0^2}}. \tag{3}$$

This solution exists, i.e., k_z is real, as long as $w_0 > 2c/\omega n_0 = 2\lambda/\pi n_0$. Since it holds directly for the Helmholtz equation, it is valid irrespective of whether the beam is plane-wave-like ($w_0/\lambda \gg 10$), paraxial ($w_0/\lambda \sim 10$), or nonparaxial

*eugenio.delre@uniroma1.it

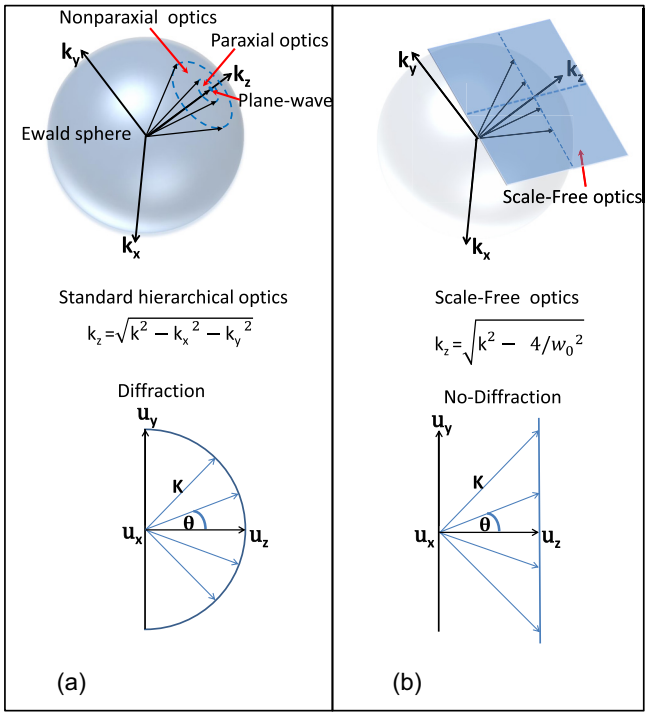

FIG. 1. (Color online) Comparing standard optics and scale-free optics. In the **k**-vector space, the plane-wave, the paraxial, and nonparaxial regimes can be schematically represented as regions of respectively increasing surface in the Ewald sphere $\mathbf{k}\cdot\mathbf{k} = (2\pi/\lambda)^2$ (top, a). Different plane-wave components emerging from a pointlike source have different phase velocities along a given direction of propagation $\mathbf{u}_z$, since their projection k_z is different. This causes diffraction (bottom, a). In the scale-free regime, in turn, the allowed **k** vectors are on a plane orthogonal to the propagation direction k_z (top, b), so that k_z does not depend on the angle of the plane-wave components with respect to the z axis, and the wavefront suffers no diffraction (bottom, b).

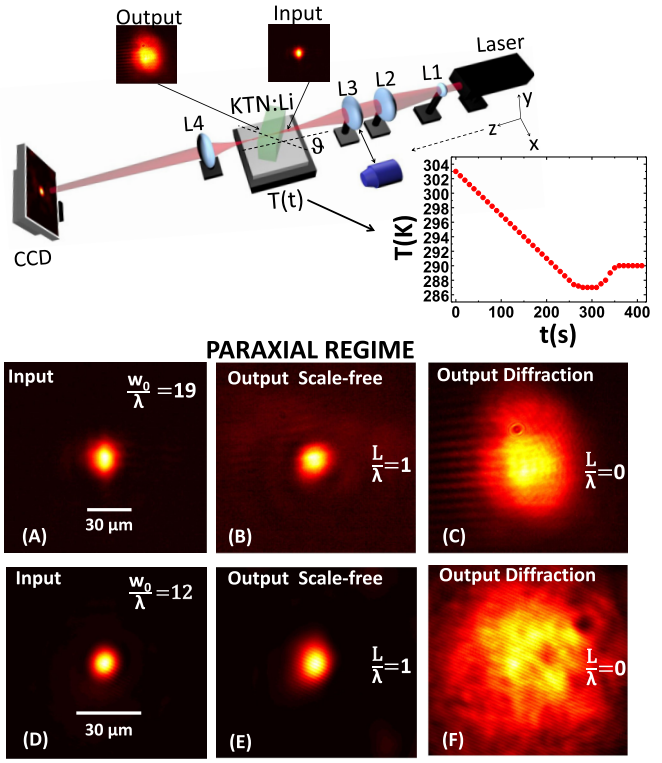

FIG. 2. (Color online) Top, experimental setup and thermal shock protocol. A He-Ne laser operating at 633 nm is enlarged through lenses L1 and L2 and focused down by lenses (paraxial case) or microscope objectives (nonparaxial case) L3 at the input facet of the KTN:Li sample, rotated with the respect to the propagation axis z by a variable angle θ and brought through a temperature cycle $T(t)$. The input and output facets are imaged through lens L4 onto a Charged Coupled Device (CCD) camera. Bottom, paraxial scale-free propagation. In the highly paraxial regime ($w_0/\lambda \gg 10$), the 12-μm Gaussian beam input (a) is compared with the 13-μm scale-free output waist ($L/\lambda = 1$) (b) and the 27-μm diffraction output ($L/\lambda = 0$) (c). Analogously, in a weaker paraxial condition ($w_0/\lambda \sim 10$), the input 7.8-μm Gaussian beam (d) is compared to the 9-μm scale-free output waist ($L/\lambda = 1$) (e) and the 38-μm diffraction output ($L/\lambda = 0$) (f). The input power in (a)–(d) cases is 800 μW.

($w_0/\lambda \sim 1$) (scale invariant). We recall that a simplified recursive approach to the photorefractive model suggests that the $\nabla I/I$ dependence for the photorefractive static electric field $\mathbf{E}_{dc}$ can hold also for narrow beams ($w_0/\lambda \sim 1$) with a strong gradient of the intensity, where charge limitation plays a role (see Eqs. (1)–(4) in the Supplementary Information of Ref. [7]). This approach must eventually break down as the beam get ever tighter, as it implies that there is no ultimate limit to the amplitude of the diffusive field. The comparison between standard optics and scale-free optics is schematically represented in Fig. 1.

III. EXPERIMENTS

To demonstrate this scale invariance, we carry out experiments with the setup illustrated in Fig. 2. A 0.8-mW (measured before L3) He-Ne laser operating at $\lambda = 632.8$ nm is expanded (L1 and L2) and subsequently focused (L3) down to a spot at the input face of a sample of lithium-enriched potassium-tantalate-niobate (KTN:Li), using spherical lenses (for the paraxial regime) or microscope objectives (for the nonparaxial regime).

The sample, a disordered ferroelectric crystal, is grown through the top-seeded solution method so as to have a peak dielectric maximum T_m at room temperature and high optical quality [20]. The crystal is a zero-cut $2.6\times3.0\times6.0$ mm sample with a composition of $K_{1-x}Ta_{1-y}Nb_yO_3 : Li_x$ with $x = 0.003$, $y = 0.36$. Cu impurities (~0.001 atoms per mole) support photorefraction in the visible range, whereas focusing and cross-polarizer experiments give $n_0 = 2.2$ and $g = 0.14$ m^4 C^{-2}. The beam is polarized in the x direction and propagates inside the crystal for a distance of $L_z \simeq 3.0$ mm. The crystal is rotated to a desired angle θ in the x,z plane. The output intensity distribution of the beam is imaged by a CCD camera through an imaging lens (L4, NA $\simeq 0.35$). The $L = \lambda$ condition forms during a transient by operating near $T_m = 287.5$ K, identified through dielectric constant measurements, using a specific thermal shock protocol [21–26] shown in Fig. 2 (top). The crystal was first cleaned of photorefractive space charge by illuminating it with a microscope illuminator. Using

a temperature controller that drives the current of a Peltier junction placed directly below the crystal in the y direction, we brought the sample to thermalize at $T_A = 303$ K. The sample is then cooled from $T_A = 303$ K at the rate of 0.06 K/s to a temperature $T_D = 287$ K, where it is kept for 60 s. Then the sample is heated once again at a rate of 0.1 K/s to the operating temperature ($>T_D$) $T_B = 290$ K. The crystal is kept in air at atmospheric pressure and is subjected to a temperature gradient orthogonal to the beam propagation (z-x plane) caused by the Peltier junction placed below the sample, on the x-z lower facet. The thermal gradient pins the polar nanoregions inducing a polarization selective nonlinearity. Hence, in our sample we are limited to a scale-free regime for x-polarized beams [7]. Once T_B is reached, the temperature cycle $T(t)$ is complete and we switched on the laser beam, recording front view images of the captured intensity distribution. The strong transient response is observed to have a characteristic response time of 10–30 s. The time scale of the transition into the diffraction cancellation regime starting from the diffractive regime is, in our conditions, approximately peak intensity independent. This means that the time dynamics are associated to the relaxation of the metastable dipolar state while the photorefractive buildup is faster and the space-charge field is at all times at steady state. We estimate the value of L by measuring the output and input waist ratio; when this ratio reaches unity we have $L \simeq \lambda$. An independent evaluation of L can ideally be obtained through time-resolved dielectric constant measurements at low frequencies of χ (and hence χ_{PNR}). However, measurements will only capture an averaged value of the χ_{PNR}, which, in proximity of the peak, leads naturally to a lower value of the enhanced dielectric constant and a diffused peak.

In Fig. 2 (bottom) we report scale-free propagation for paraxial beams. As shown in Figs. 2(a)–2(c) the $w_0 = 12$ μm ($w_0/\lambda = 19$) input beam diffracts to 27 μm as it propagates to the output facet at the initial $T_A = 303$ K. After the cooling and heating cycle, the output beam shrinks to 13 μm. Analogously in Figs. 2(d)–2(f), the $w_0 = 7.8$ μm ($w_0/\lambda = 12$) input beam diffracts to 38 μm as it propagates to the output facet at the initial $T_A = 303$ K. After the cooling-heating cycle, the output beam shrinks to 9 μm. Overall confirmation that this is associated to diffraction-free propagation all along the sample is provided by top-view images of scattered light (not included here), as described in other reports [7,16]. Limited resolution, however, does not exclude the possibility of localized and partial overfocusing and antidiffraction. In Fig. 3 we report scale-free propagation for the nonparaxial beams. In Figs. 3(a)–3(c), a $w_0 = 1.5$ μm input beam ($w_0/\lambda = 2.4$) is launched directly from a zero-working-distance immersion microscope objective (numerical aperture [NA] of 0.8, used without oil with $\theta = 0$) placed at the input face of the sample. After we enacted the thermal cycle (in the scale-free regime) we measured a 1.7-μm output waist. In Figs. 3(d)–3(f), the narrower input beam with $w_0 = 0.49$ μm ($w_0/\lambda = 0.8$) is achieved using a fully illuminated long-working-distance dry objective (Edmund Optics $\times 100$, NA 0.8, $\theta = 11^\circ$ to avoid the effect of growth-related striations). After we enacted the thermal cycle, we measured a 0.66-μm output waist. The beam width is measured using a knife-edge technique in proximity to the input plane, from the transmitted power plot [Figs. 3(g) and 3(h)] by fitting the data with what is expected for a two-dimensional Gaussian beam intensity shape of width w_0. In detail, we mounted a plate on a 3-axis nanopositioning stage, aligned it to the plane orthogonal to the laser propagation axis z, and placed it in proximity of the output plane of the objective, to a precision below 1 μm (this is required because the confocal parameter of the beam is on the order of tens of micrometers). The power of the transmitted light as a function of the lateral x displacement of the plate edge was then detected using a silicon-head power meter. In Fig. 4 we combine results and illustrate in full the breaking of the conventional optical spatial hierarchy. Even though limits associated with charge saturation and the transient nature of the effect require further analysis, we note that our findings could form the basis for super-resolved imaging. In fact, in standard optical propagation a finite angular spread implies loss of original resolution during propagation and hence a distortion of images. The diffraction-cancellation regime allows the preservation of the spatial resolution of light emitted from a plane as it propagates to collecting optics. Hence, in principle, we can interpose a slab of KLTN in between the objective of the microscope and the sample to analyze. The increase in depth of focus for a fixed collecting numerical aperture amounts to an increase of the overall effective resolution. For example, a visible pixel ceases to represent an independent source of information when it becomes equal to or smaller than a micrometer, in which case $\Delta\theta \sim 1$, and its emission is mingled with that of other pixels after just a few micrometers of

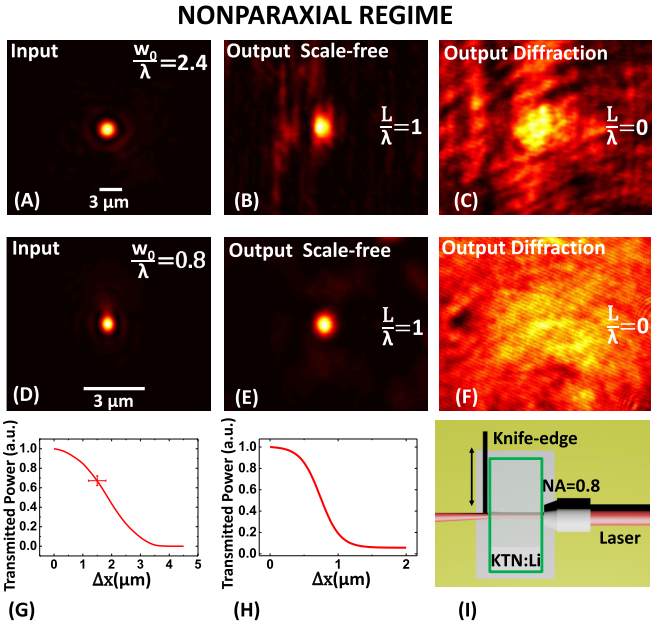

FIG. 3. (Color online) Nonparaxial scale-free propagation. A nonparaxial $w_0 = 1.5$ μm ($w_0/\lambda = 2.4$) beam input (a) is compared with the 1.7-μm scale-free output waist ($L/\lambda = 1$) (b) and the >60-μm greatly delocalized output ($L/\lambda = 0$) (c). Analougously, in the highly nonparaxial condition ($w_0/\lambda = 0.8$), the input 0.49-μm beam (d) is compared with the 0.66-μm scale-free output waist ($L/\lambda = 1$) (e) and the >90-μm delocalized output ($L/\lambda = 0$) (f). (g)–(h) Knife-edge scan for (a) and (d) cases. (i) Knife-edge scheme for output distributions. The input power in (a)–(d) cases is 800 μW.

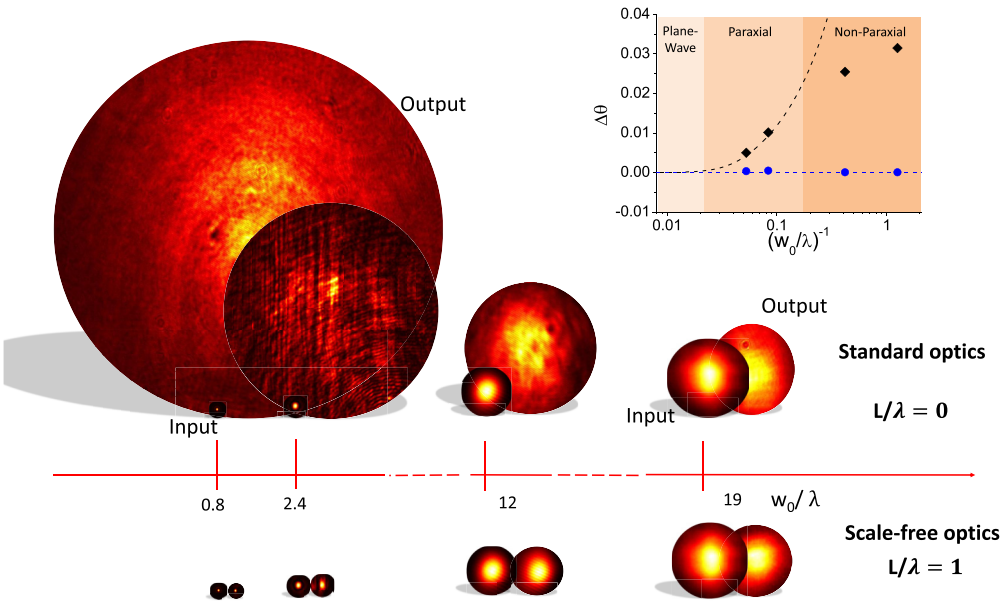

FIG. 4. (Color online) Scale-invariance: the full picture. Comparison of input vs output beam intensity distribution (see inset) in the standard optics regime ($L/\lambda = 0$, top sequence) and in the scale-free-optics regime ($L/\lambda = 1$, bottom sequence), as function of w_0/λ. The use of a single common spatial scale illustrates the fundamental difference between the standard scale hierarchy (top) and scale-free case (bottom) across the entire span of optical regimes, i.e., from plane waves to nonparaxial waves.

propagation. No such distortion will occur if the pixels were to transmit light in a system supporting scale-free optics. In turn, conventional techniques based on diffraction compensation through wave guides or spatial solitons are limited to paraxial beams [27–29].

IV. CONCLUSIONS

To sum up, although Maxwell's equations are free of any spatial scale, in all practical devices this scale symmetry is broken by the wavelength λ around which a specific device operates. The wavelength introduces a hierarchy of different propagation phenomena as measured in terms of the ratio between the light beam width w_0 and λ, as quantified by the angular spread of the beam $\Delta\theta$. Starting from the quasimonochromatic reduction of the electromagnetic wave equation, we can distinguish a so-called nonparaxial regime described by the Helmholtz equation for $w_0/\lambda \sim 1$, a paraxial regime described by the parabolic propagation equation for $w_0/\lambda \sim 10$, and a plane-wave geometrical optics regime for $w_0/\lambda \gg 10$. In a diffusive nonlinearity supported by a nanodisordered photorefractive ferroelectric crystal, we are able to observe beams without diffraction independently of size and intensity across the entire span of these commonly accepted wave-propagation regimes, that is, from what would be plane waves to nonparaxial (spherical) waves. In other words, in our material, all light beams obey geometrical-optics-like laws.

ACKNOWLEDGMENTS

Funding from Grants No. PRIN 2012BFNWZ2 and No. Sapienza 2013, are acknowledged. A.J.A. acknowledges the support of the Peter Brojde Center for Innovative Engineering.

[1] M. Born and E. Wolf, *Principles of Optics*, 6th ed. (Pergamon Press, Oxford, 1980).
[2] S. Nemoto, Appl. Opt. **29**, 1940 (1990).
[3] H. Kosaka, T. Kawashima, A. Tomita, M. Notomi, T. Tamamura, T. Sato, and S. Kawakami, Appl. Phys. Lett. **74**, 1212 (1999).
[4] H. S. Eisenberg, Y. Silberberg, R. Morandotti, and J. S. Aitchison, Phys. Rev. Lett. **85**, 1863 (2000).
[5] K. Staliunas and R. Herrero, Phys. Rev. E **73**, 016601 (2006).
[6] O. Firstenberg, P. London, M. Shuker, A. Ron, and N. Davidson, Nat. Phys. **5**, 665 (2009).
[7] E. DelRe, E. Spinozzi, A. J. Agranat, and C. Conti, Nat. Photon. **5**, 39 (2011).
[8] D. N. Christodoulides and T. H. Coskun, Opt. Lett. **21**, 1460 (1996).
[9] B. Crosignani, E. DelRe, P. Di Porto, and A. Degasperis, Opt. Lett. **23**, 912 (1998).
[10] B. Crosignani, A. Degasperis, E. DelRe, P. DiPorto, and A. J. Agranat, Phys. Rev. Lett. **82**, 1664 (1999).
[11] E. DelRe, M. Tamburrini, M. Segev, R. Della Pergola, and A. J. Agranat, Phys. Rev. Lett. **83**, 1954 (1999).
[12] C. Conti, A. J. Agranat, and E. DelRe, Phys. Rev. A **84**, 043809 (2011).
[13] J. Parravicini, F. Di Mei, C. Conti, A. J. Agranat, and E. DelRe, Opt. Exp. **19**, 24109 (2011).
[14] E. DelRe and C. Conti, in *Nonlinear Photonics and Novel Optical Phenomena*, edited by Z. Chen and R. Morandotti (Springer, New York, 2012).
[15] V. Folli, E. DelRe, and C. Conti, Phys. Rev. Lett. **108**, 033901 (2012).

[16] F. Di Mei, J. Parravicini, D. Pierangeli, C. Conti, A. J. Agranat, and E. DelRe, Opt. Exp. **22**, 31434 (2014).
[17] E. DelRe, F. Di Mei, J. Parravicini, G. B. Parravicini, A. J. Agranat, and C. Conti, Nat. Photon. **9**, 228 (2015).
[18] A. A. Bokov and Z.-G. Ye, J. Mater. Sci. **41**, 31 (2006).
[19] A. Gumennik, Y. Kurzweil-Segev, and A. J. Agranat, Opt. Mater. Express **1**, 332 (2011).
[20] A. Agranat, R. Hofmeister, and A. Yariv, Opt. Lett. **17**, 713 (1992).
[21] Y-C. Chang, C. Wang, S. Yin, R. C. Hoffman, and A. G. Mott, Opt. Lett. **38**, 4574 (2013).
[22] Y.-C. Chang, C. Wang, S. Yin, R. C. Hoffman, and A. G. Mott, Opt. Express **21**, 17760 (2013).
[23] J. Parravicini, C. Conti, A. J. Agranat, and E. DelRe, Opt. Lett. **37**, 2355 (2012).
[24] J. Parravicini, A. J. Agranat, C. Conti, and E. DelRe, Appl. Phys. Lett. **101**, 111104 (2012).
[25] J. Parravicini, D. Pierangeli, F. DiMei, A. J. Agranat, C. Conti, and E. DelRe, Opt. Express **21**, 30573 (2013).
[26] D. Pierangeli, J. Parravicini, F. DiMei, G. B. Parravicini, A. J. Agranat, and E. DelRe, Opt. Lett. **39**, 1657 (2014).
[27] R. W. Boyd, S. G. Lukishova, and Y. R. Shen, *Self-Focusing: Past and Present* (Springer, New York, 2009).
[28] S. Trillo and W. Torruellas (eds.), *Spatial Solitons* (Springer, Berlin, 2001).
[29] Z. G. Chen, M. Segev, and D. N. Christodoulides, Rep. Prog. Phys. **75**, 086401 (2012).